Supporting Information (ESI)

Supramolecular Bimetallogels: A Nanofiber Network for Bimetal/Nitrogen Co-Doped Carbon Electrocatalysts

Minli Tan,[a] Ting He,[a] Jian Liu,[a] Huiqiong Wu,[a] Qiang Li,[a] Jun Zheng,[a] Yong Wang,[a] Zhifang Sun,*[a] Shuangyin Wang,[b] and Yi Zhang*[a]

[a.] *Hunan Provincial Key Laboratory of Efficient and Clean Untilization of Manganse Resources, College of Chemistry and Chemical Engineering, Central South University, Changsha 410083, China. E-mail: allensune@gmail.com (Z. Sun); yzhangcsu@csu.edu.cn (Y. Zhang)*

[b.] *State Key Laboratory of Chem/Bio-Sensing and Chemometrics, Hunan University, Changsha 410082, China*

1. Instruments

Scanning electron microscopic (SEM) images were acquired on a Hitachi S-4800 SEM (Japan) with an accelerating voltage of 10 kV. Transmission electron microscopic (TEM) images were obtained from a T20 FEI TECNA1 G2 (USA). High-angle annular dark field scanning TEM (HAADF-STEM) images and HAADF-STEM energy dispersive X-ray spectroscopy (HAADF-STEM-EDS) maps were recorded on a FEI Titan G2 60-300 (USA). Circular dichroism (CD) spectra of different samples were recorded by using Jasco-815 CD spectrometer (Japan). Fourier transform infrared spectroscopy (FT-IR) was acquired with a Perkin Elmer Spectrum One instrument (USA). X-ray photoelectron spectra (XPS) were obtained from an ESCALAB 250Xi X-ray photoelectron spectrometer (USA). The C 1s line at 284.8 eV was used to calibrate the positions of all binding energies. X-ray powder diffraction (XRD) was carried out at D/max 2550 power diffractometer (Japan) using a graphite-filtered Cu Kα radiation manipulating at 40 kV. Voltammetry tests were performed on the RST 5200F electrochemical workstations (China). Rotating disk electrode (RDE) measurements were employed on a MSR speed controller of Pine Research Instrumentation (USA) and Zahner electrochemical workstations (Germany).

2. Catalyst synthesis

2.1 Synthesis of Fc-F. The Fc-F was synthesized as described in our previous work.[1]

2.2 Synthesis of Fc-F/Co@N-C150 nanocomposites. A certain amount of Fc-F stock solution (200 mM, in DMSO), cobalt acetate stock aqueous solution (200 mM, ph~7), and Ketjenblack EC 600J (EC) were added into deionized water. After sonication for 20 minutes, the Fc-F/Co and carbon black co-assembled into hybrid bimetallogel Fc-F/Co@C. Final concentrations of Fc-F, Co^{2+} and EC in the hybrid bimetallogel were 20 mM, 20 mM and 0.7 mg mL^{-1}, respectively. The well-dispersed black gel was transferred into a Teflon autoclave and allowed by hydrothermal treatment at 150 °C for 12 h. The obtained product was collected by centrifugation (5000 rpm for 5 min), and then washed with water to remove impurities. After freeze-drying, Fc- bimetal nanocomposite Fc-F/Co@N-C150 were prepared. Likewise, Fc-F/Ni@N-C150, Fc-F/Mn@N-C150 were prepared in similar way.

2.3 Synthesis of Fc-F/Co@N-C800 derived from Fc-F/Co@N-C150. The Fc-F/Co@N-C150 nanocomposite was calcined at 800 °C with a rate of 10 °C min^{-1} in an argon atmosphere for 2 h. Moreover, by replacing cobalt acetate with manganese chloride and nickel chloride, Fc-F/TM@N-C800 (TM=Mn, Ni) catalysts can be prepared. The synthesis procedure of Fc-F@N-C800 and Co@N-C800 control samples are similar to the Fc-F/Co@N-C800 product except for without adding Fc-F and Co^{2+} into the precursor solution, respectively. Likewise, another control sample, C800, was prepared by using the same approach as that employed for the synthesis of Fc-F/Co@N-C800 except for adding no metal sources into the precursor solution.

2.4 Synthesis of Fc/Co@N-C800 and Fe/Co@N-C800. The Fc/Co@N-C800 and Fe/Co@N-C800 were obtained by using the same approach as that employed for the synthesis of Fc-F/Co@N-C800, but in these cases ferrocene and iron chloride were used instead of Fc-F, respectively.

3. Electrochemical measurements

All the electrochemical measurements were performed in a conventional three-electrode electrochemical cell in a 0.1 M KOH (or 0.1 M $HClO_4$) electrolytic solution using a glassy carbon electrode as the working electrode, a Pt wire (Pt plate for RDE test) as the counter electrode, and Ag/AgCl electrode (saturated KCl) as the reference electrode. N_2 or O_2 was used to adjust oxygen-free or oxygen-filled environments. Potential measured was converted to the reversible hydrogen electrode (RHE) value in line with Nernst equation as follows: $E_{RHE} = E_{Ag/AgCl} + 0.2089 + 0.05916pH$ V (at 15 °C).

For CV tests, 2 mg catalysts (or commercial 20% Pt/C) were dispersed in 1 mL of mixed solvent (water : isopropanol = 1:1; *V/V*) with 10 μL of nafion by ultrasound treatment for 30 min to form a homogeneous black solution. 7 μL of the well-dispersed catalyst ink was dropped onto the 3-mm glassy carbon electrode surface (the catalyst loading: 0.20 mg cm^{-2}). For RDE tests, 19.6 μL of ink was dropped onto the 5-mm glassy carbon electrode surface to obtain the same catalyst loading. All RRDE measurements were carried out at a rotation speed of 1600 rpm. The CV curves were obtained at a scan rate of 50 mV s^{-1}. The LSV curves were obtained at a scan rate of 5 mV s^{-1}.

The stability test was carried out at room temperature before and after 3000 cycles at a rate of 100 mV s^{-1}. At the end of the cycles, the consequent electrode was used for CV at a scan rate of 50 mV s^{-1}. Chronoamperometry was measured at 0.678 V for 40000 s in O_2-satured 0.1 M KOH.

For the electrical impedance spectra, the frequency range was 0.01 Hz to 1000 kHz.

For Al-air full battery test, aluminium plate was used as the anode and 6 M KOH consisting of 0.01 M Na_2SnO_3, 0.0005 M $In(OH)_3$, 0.0075 M ZnO as corrosion inhibitors. The air electrode was composed of gas diffusion layer, current collector and the catalytic layer. Nickel foam was employed as the current collector owing to its good conductivity and intense strength. The catalytic layer was constructed as follows: Fc-F/Co@N-C800, active acetylene black, polytetrafluoroethylene (PTFE) in a weight ratio of 6:1:3 were mixed well firstly, and then the paste was rolled into sheets with a thickness of ~0.2 mm. Finally, the film and gas diffusion layer were pressed onto the two sides of nickel foam, respectively, and then dried at 60 °C for 12 h.

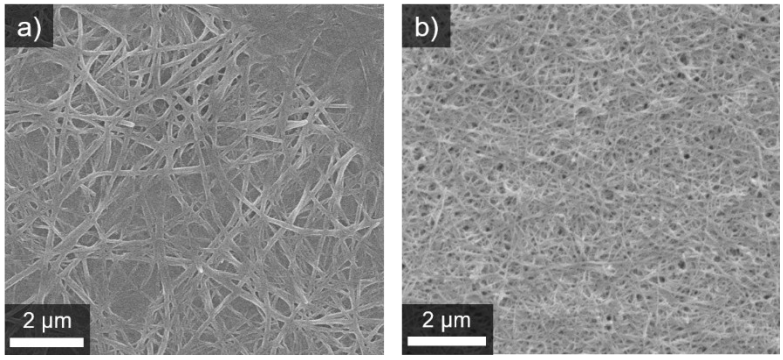

Fig. S1 SEM images of different hydrogels. (a) Fc-F hydrogel; (b) Fc-F/Co hydrogel, respectively.

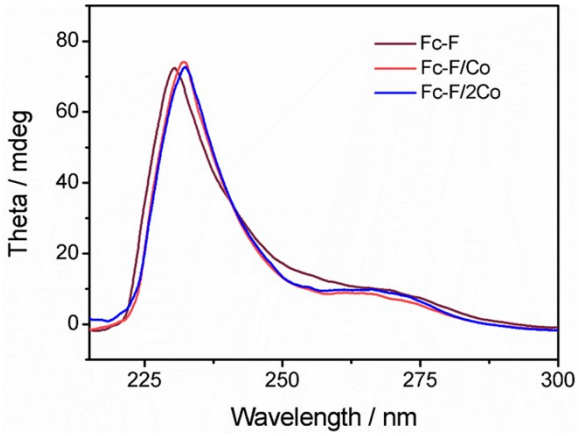

Fig. S2 CD signals for Fc-F (black line), Fc-F/Co (red line), and Fc-F/2Co (blue line). The number "2" represents molar ratio.

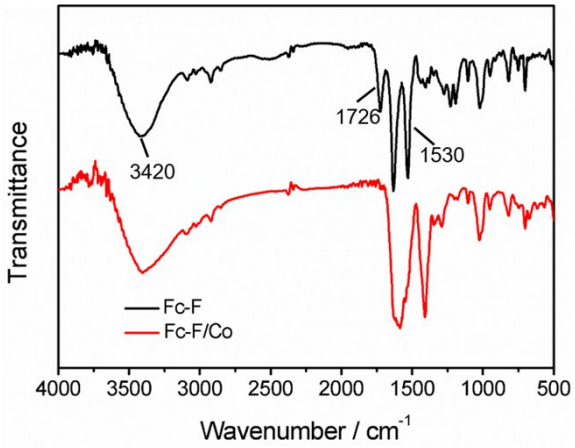

Fig. S3 FT-IR spectra of the Fc-F and Fc-F/Co gels.

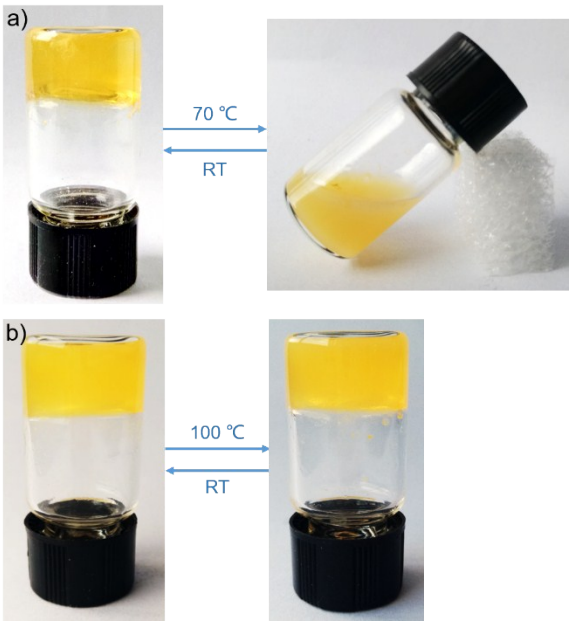

Fig. S4 Reversible gel−sol transitions of the supramolecular metallogel triggered by temperature. (a) Fc-F, (b) Fc-F/Co.

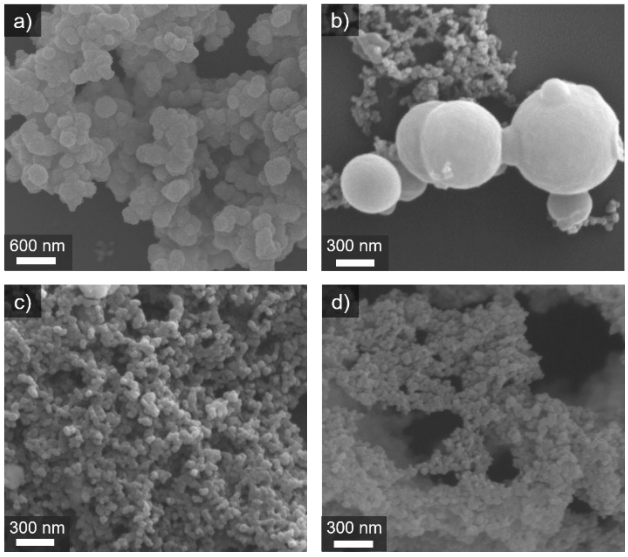

Fig. S5 SEM images of (a) Fc-F/Co@N-C150, (b) Fc-F@N-C150, (c) Co@N-C150, and (d) C150, respectively.

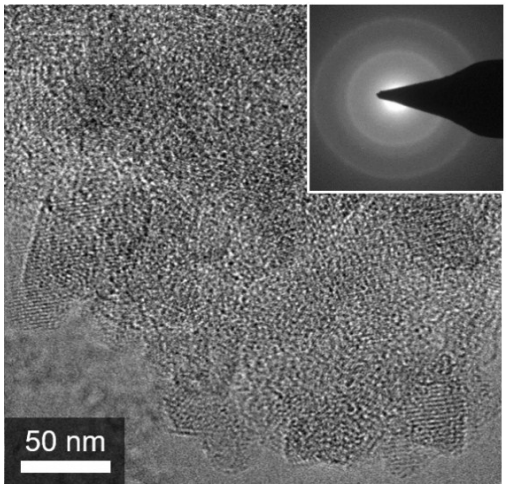

Fig. S6 HRTEM image of raspberry-like Fc-F/Co@N-C150. The inset shows the selected area electron diffraction (SAED) pattern.

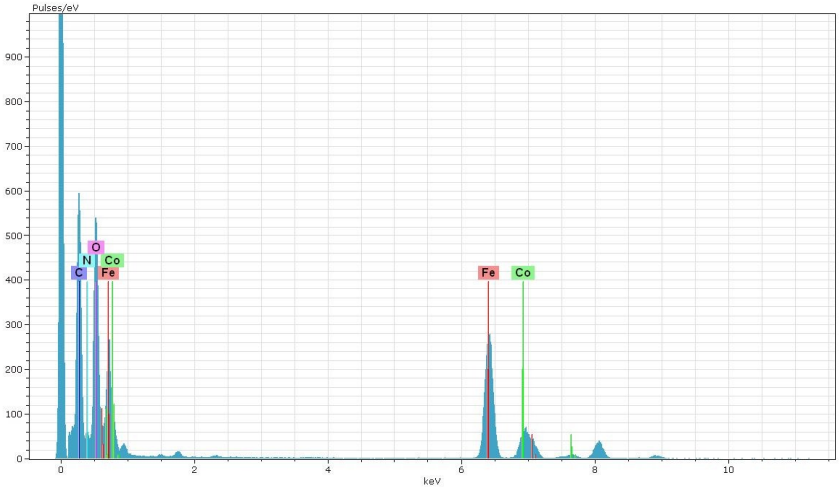

Fig. S7 The energy dispersive X-ray spectra of the raspberry-like Fc-F/Co@N-C150.

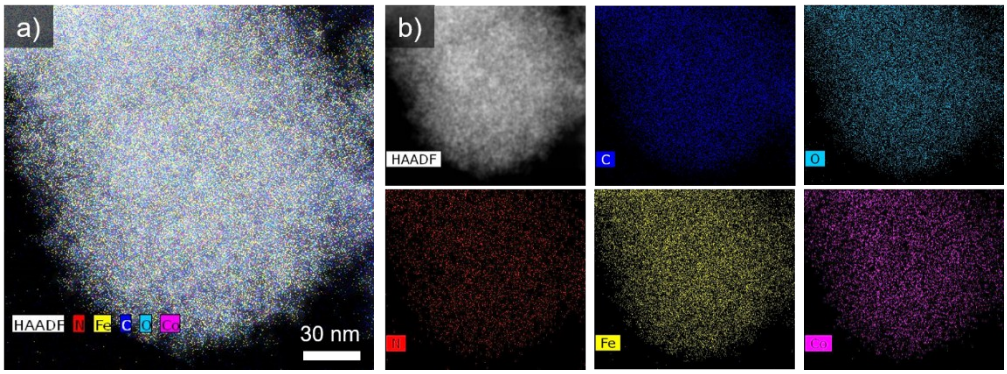

Fig. S8 The HAADF-STEM images and the HAADF-STEM-EDS maps of raspberry-like Fc-F/Co@N-C150.

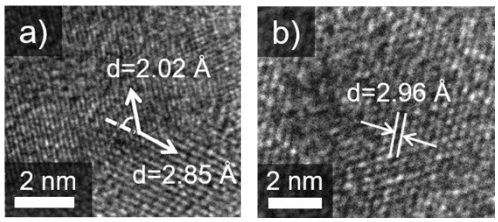

Fig. S9 HRTEM images of the Fc-F/Co@N-C800, and the lattice distance and crystal plane angle indicate the coexistence of FeCo and $CoFe_2O_4$ nanoparticles.

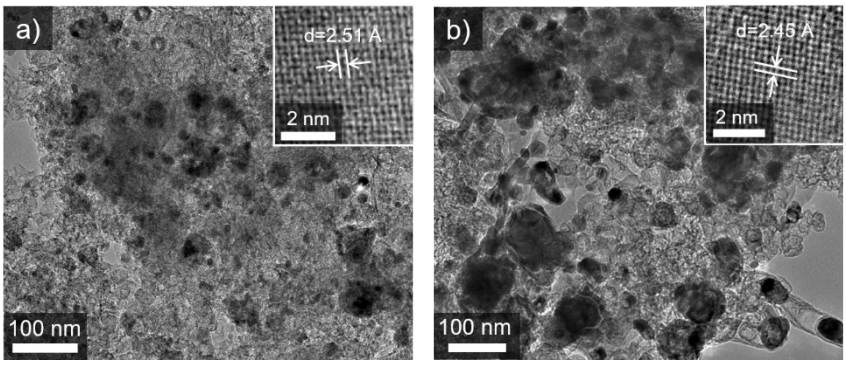

Fig. S10 TEM images of (a) Fc-F@N-C800, (b) Co@N-C800, respectively. The corresponding metal nanoparticles and the index crystal planes are shown in the insets.

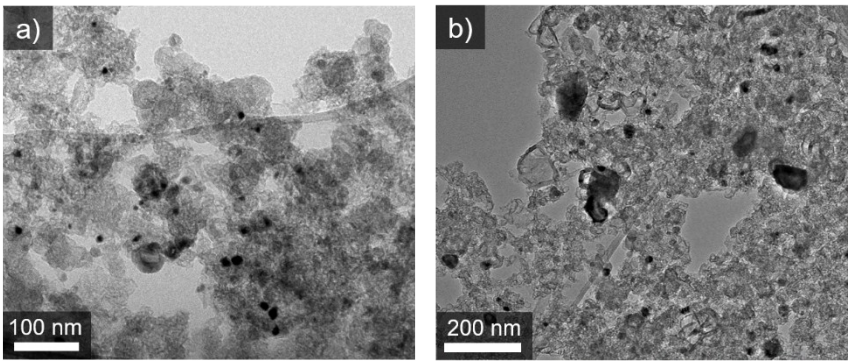

Fig. S11 TEM images of as-prepared Fc-F/Co@N-C at (a) 700 ° C, (b) 900 ° C, respectively.

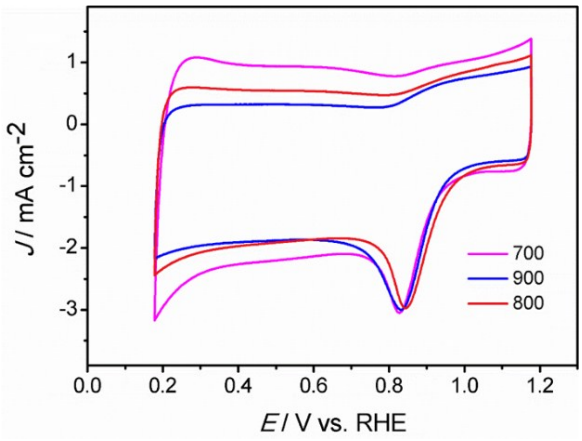

Fig. S12 CV curves of as-prepared Fc-F/Co@N-C materials at different pyrolysis temperatures in O_2-saturated 0.1 M KOH. Scan rate: 50 mV s^{-1}.

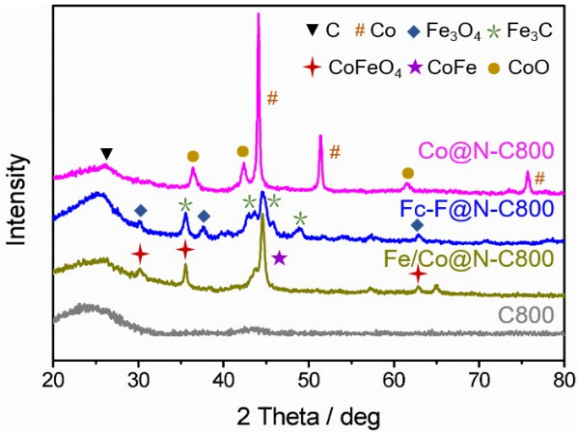

Fig. S13 XRD patterns of Fc-F@N-C800, Co@N-C800, Fe/Co@N-C800 and C800.

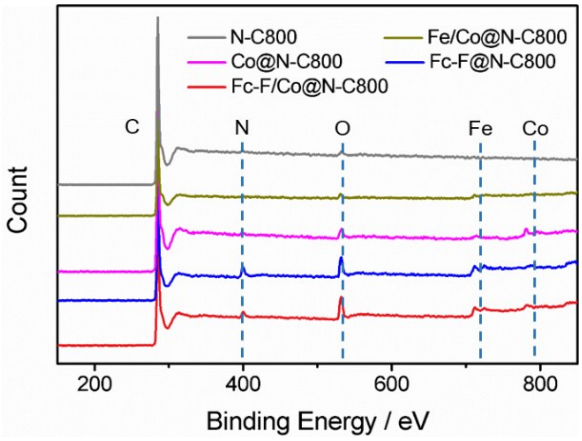

Fig. S14 Survey spectra of the as-prepared materials.

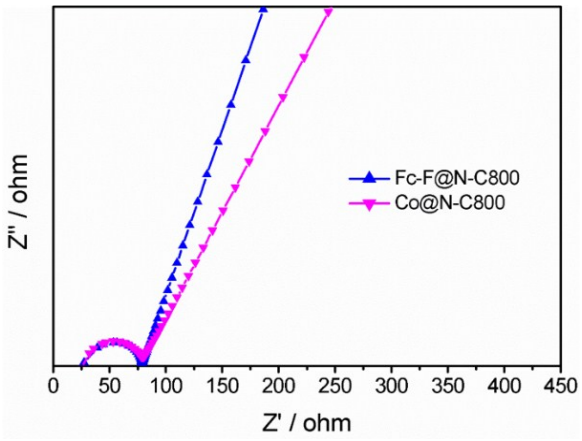

Fig. S15 Nyquist plots of as-prepared materials.

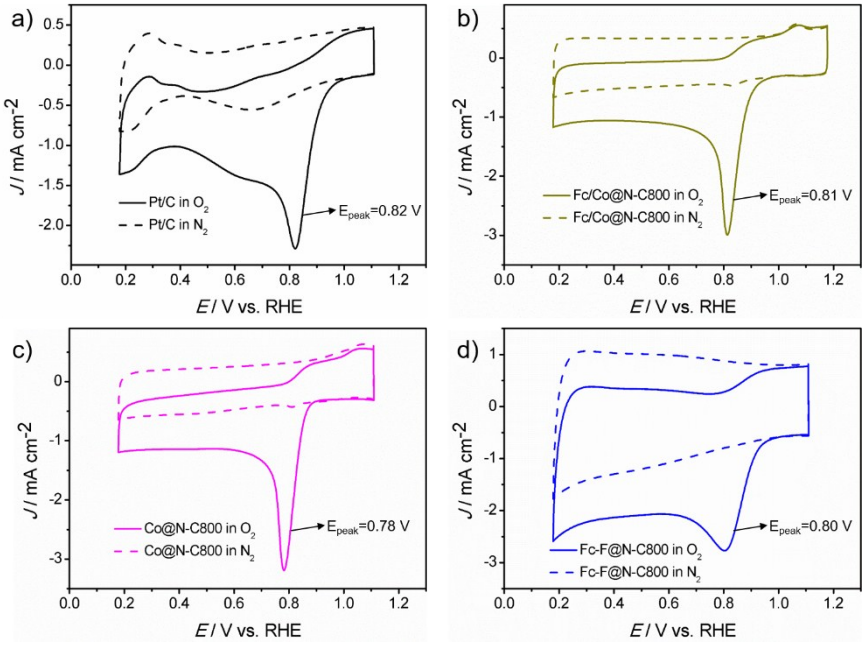

Fig. S16 CV curves of as-prepared catalysts in 0.1 M KOH. Scan rate: 50 mV s^{-1}.

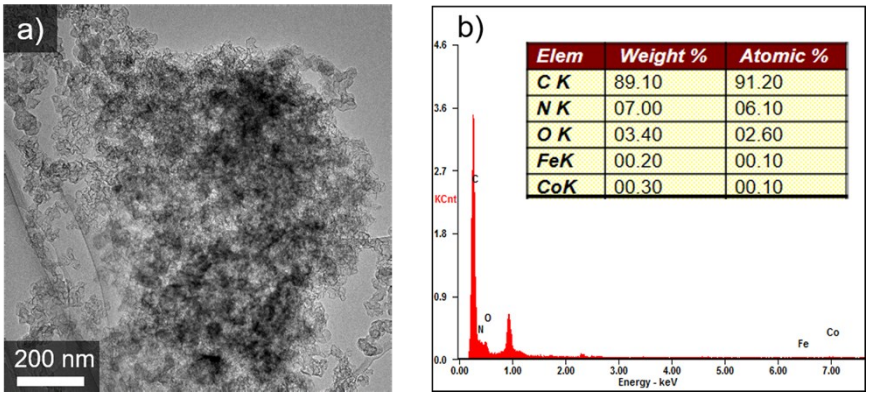

Fig. S17 (a) TEM image and (b) EDS of Fc-F/Co@N-C800 catalyst after acid leaching.

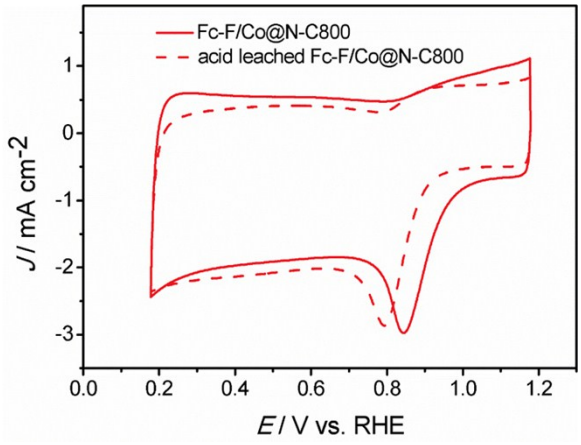

Fig. S18 CV curves of as-prepared and acid-leached Fc-F/Co@N-C800. Scan rate: 50 mV s^{-1}.

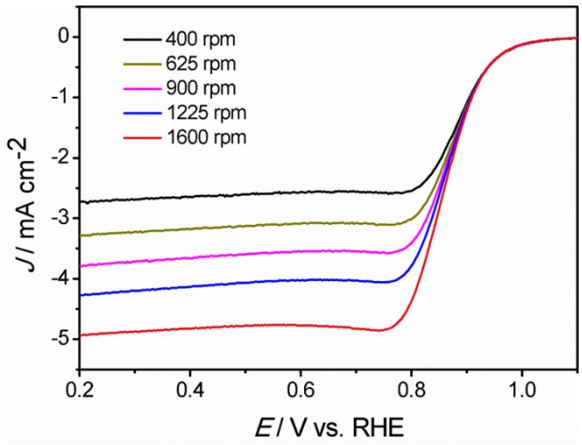

Fig. S19 Polarization curves of Fc-F/Co@N-C800 at different rotation rates.

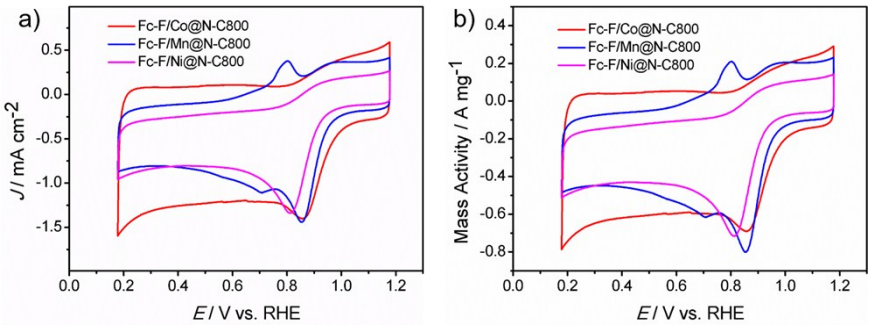

Fig. S20 (a) CV curves and (b) Mass activity of Fc-F/M@N-C800 (M=Co, Ni, Mn). Scan rate: 20 mV S^{-1}, loading mass: 0.2 mg cm^{-2}.

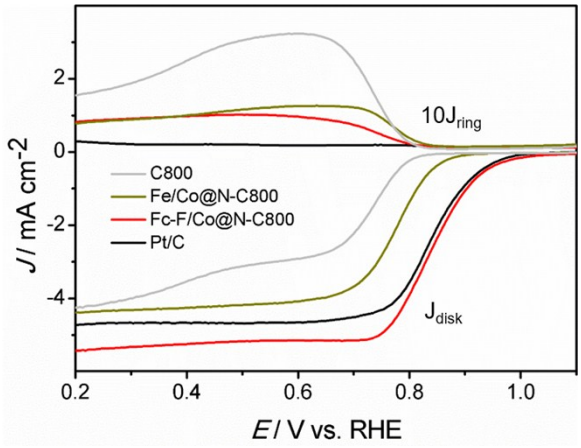

Fig. S21 RRDE voltammograms of the as-prepared materials. Rotation rates: 1600 rpm, scan rate: 5 mV S^{-1}, loading mass: 0.2 mg cm^{-2}.

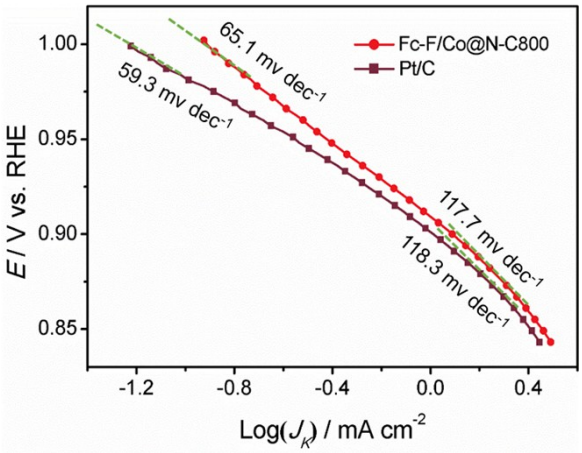

Fig. S22 Tafel plots of Fc-F/Co@N-C800 and 20 wt% Pt/C.

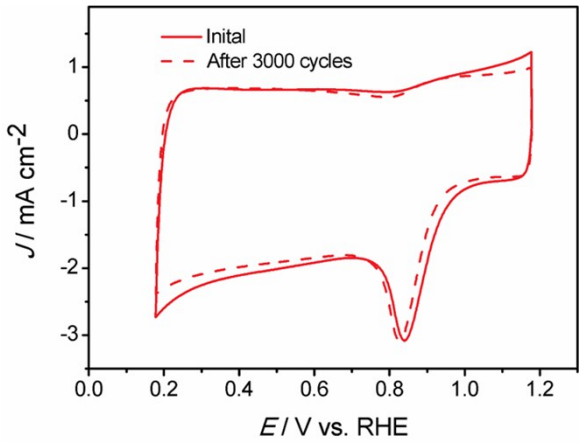

Fig. S23 Cycling durability test of Fc-F/Co@N-C800 catalyst in O_2-saturated 0.1 M KOH.

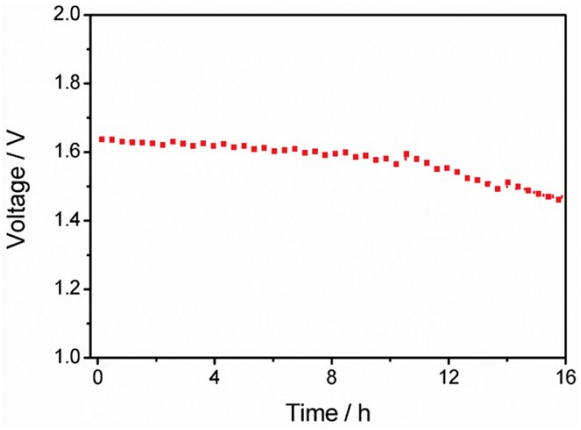

Fig. S24 Constant current discharge test for Al-air battery at a discharge current density of 20 mA cm^{-2}.

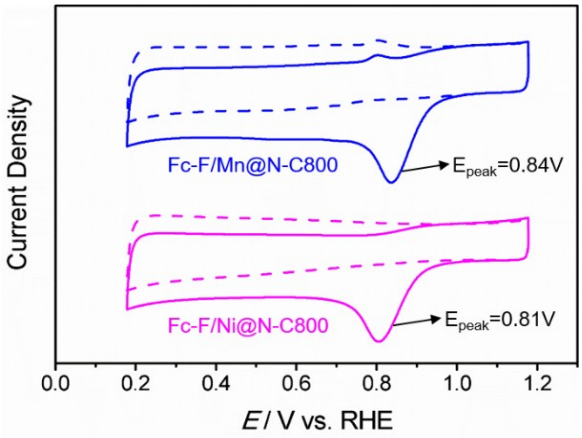

Fig. S25 CV curves of as-prepared Fc-F/Mn@N-C80 and Fc-F/Ni@N-C800 in 0.1 M KOH. Scan rate: 50 mV s^{-1}.

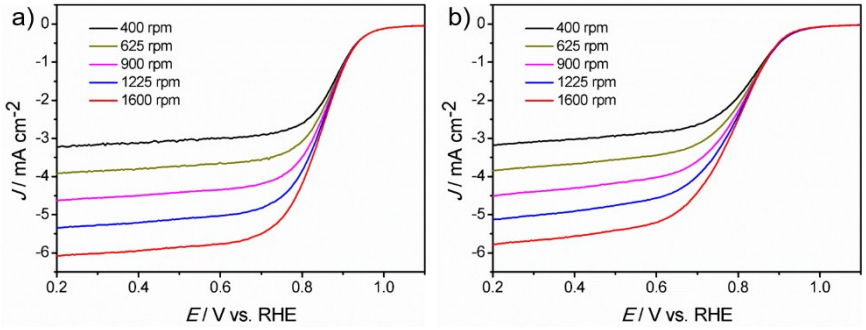

Fig. S26 Polarization curves of as-prepared Fc-F/Mn@N-C800 and Fc-F/Ni@N-C800 at different rotation rates.

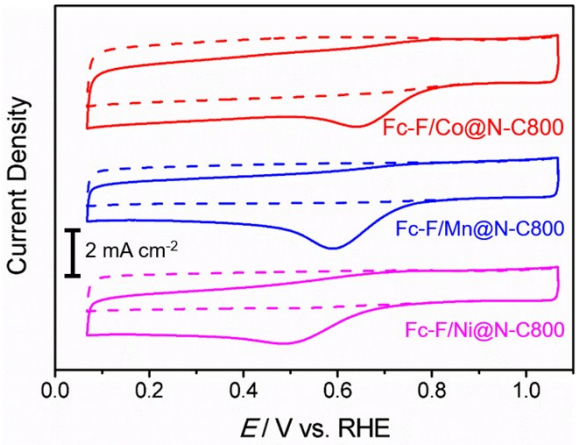

Fig. S27 CV curves of Fc-F/M@N-C800 (M=Co, Mn, Ni) catalysts in O_2-saturated (solid line) and N_2-satureted (dash line) 0.1 M $HClO_4$. Scan rate: 50 mV s^{-1}.

Table S1 Elements distribution of the as-prepared materials from XPS.

Catalysts	C / at%	N / at%	O / at%	Fe / at%	Co / at%	Active N / at%
Fc-F@N-C800	86.08	5.79	6.44	1.7		5.44
Co@N-C800	95.75	1.06	2.59		0.6	0.95
Fe/Co@N-C800	95.86	1.23	1.88	0.14	0.88	0.91
Fc-F/Co@N-C800	88.85	3.14	7.01	0.23	0.77	2.75

Table S2 The calculated EIS results of C800, Fe/Co@N-C800, Co@N-C800, Fc-F@N-C800, and Fc-F/Co@N-C800 catalysts.

Catalysts	R_s	R_{ct}	Q	C_{dl}	C_L
C800	27.03	54.62	$4.281E^{-4}$	$3.346E^{-8}$	$1.588E^{-5}$
Fc-F@N-C800	26.13	52.07	$1.508E^{-4}$	$3.169E^{-8}$	$1.541E^{-5}$
Co@N-C800	26.31	54.79	$1.356E^{-4}$	$4.668E^{-8}$	$1.706E^{-5}$
Fe/Co@N-C800	25.76	69.86	$2.861E^{-4}$	$3.129E^{-8}$	$1.694E^{-5}$
Fc-F/Co@N-C800	26.31	50.26	$3.328E^{-4}$	$3.549E^{-8}$	$1.425E^{-5}$

Table S3 The ORR catalytic performances of MNC catalysts in recent literatures (electrode rotating speed is 1600 rpm, in 0.1 M KOH solution).

Materials	Loading (mg cm^{-2})	E_{onset} (V vs. RHE)	$E_{1/2}$ (V vs. RHE)	Electron transfer numbers	Reference
Fc-F/Co@N-C800	0.2	1.01	0.86	3.89	**This work**
CoO_x NPs/BNG	N.A.	0.95	0.805	~4.0	[1]
S,N-Fe/N/C-CNT	0.6	N.A.	0.85	~4.0	[2]
$Co@Co_3O_4$/NC-1	0.21	N.A.	0.80	3.78	[3]
{Co}[FeCo]O_4/NG	0.6	0.98	0.866	3.9	[4]
Co-TA-800	0.3	0.95	N.A.	3.7-4.0	[5]
FP-Fe-TA-N-850	0.3	0.98	N.A.	3.7-3.9	[6]
CoN-CNT	N.A.	0.93	0.82	3.96	[7]
Fe_9S_{10}(700)/N,S-G	0.283	0.959	0.80	~4.0	[8]
LDH@ZIF-67-800	0.2	0.94	0.83	3.94	[9]
ZIF-67 derived NCNTF	0.2	~1.00	0.87	3.97-3.99	[10]
NCNT/$Co_xMn_{1-x}O$	0.21	0.96	0.84	~3.8	[11]
Fe/N-CNT	0.2	0.96	0.84	~3.85	[12]

Table S4 The total metal (TM) contents of Fc-F/M@N-C800 (M=Co, Mn, Ni) detected by AAS.

Catalysts	$Concentration_{Fe}$ / mg L^{-1}	$Concentration_{M}$ / mg L^{-1}	Volume / L	$Mass_{TM}$ / mg	$Mass_{Total}$ / mg	Wt %
Fc-F/Co@N-C800	0.797	0.305	0.25	0.276	1.9	14.53
Fc-F/Mn@N-C800	0.783	0.193	0.25	0.244	1.9	12.84
Fc-F/Ni@N-C800	0.658	0.357	0.25	0.254	1.9	13.37

References

[1] Y. Tong, P. Z. Chen, T. P. Zhou, K. Xu, W. S. Chu, C. Z. Wu, Y. Xie, *Angew. Chem. Int. Ed.* **2017**, *56*, 7121-7125.
[2] P. Z. Chen, T. P. Zhou, L. L. Xing, K. Xu, Y. Tong, H. Xie, L. D. Zhang, W. S. Yan, W. S. Chu, C. Z. Wu, Y. Xie, *Angew. Chem. Int. Ed.* **2017**, *56*, 610-614.
[3] A. Aijaz, J. Masa, C. Rösler, W. Xia, P. Weide, A. J. R. Botz, R. A. Fischer, W. Schuhmann, M. Muhler, *Angew. Chem. Int. Ed.* **2016**, *55*, 4087-4091.
[4] G. P. Wu, J. Wang, W. Ding, Y. Nie, L. Li, X. Q. Qi, S. G. Chen, Z. D. Wei, *Angew. Chem. Int. Ed.* **2016**, *55*, 1340-1344.
[5] J. Wei, Y. Liang, Y. X. Hu, B. Kong, J. Zhang, Q. F. Gu, Y. P. Tong, X. B. Wang, S. P. Jiang, H. T. Wang, *Angew. Chem. Int. Ed.* **2016**, 55, 12470-12474.
[6] J. Wei, Y. Liang, Y. X. Hu, B. Kong, G. P. Simon, J. Zhang, S. P. Jiang, H. T. Wang, *Angew. Chem. Int. Ed.* **2016**, 55, 1355-1359.
[7] S. Kim, D. Jang, J. Lim, J. Oh, S. O. Kim, S. Park, *ChemSusChem* **2017**, *10*, 3473-3481.
[8] X. X. Ma, Y. Su, X. Q. He, *Catal. Sci. Technol.* **2017**, 7, 1181-1192.
[9] Z. H. Li, M. F. Shao, L. Zhou, R. K. Zhang, C. Zhang, M. Wei, D. G. Evans, X. Duan, *Adv. Mater. 2016*, 28, 2337-2344.
[10] B. Y. Xia, Y. Yan, N. Li, H. B. Wu, X. W. Lou, X. Wang, *Nat. Energy 2016*, 1, 15006-15013.
[11] X. Liu, M. Park, G. K. Min, S. Gupta, X. Wang, G. Wu, J. Cho, *Nano Energy* **2016**, 20, 315-325.
[12] Y. Y. Liu, H. L. Jiang, Y. H. Zhu, X. L. Yang, C. Z. Li, *J. Mater. Chem. A* **2016**, 4, 1694-1701.